Cancer Cell
Article

Proteomic and Genetic Approaches Identify Syk as an AML Target

Cynthia K. Hahn,[1,6] Jacob E. Berchuck,[1,6] Kenneth N. Ross,[2] Rose M. Kakoza,[1] Karl Clauser,[2] Anna C. Schinzel,[2,3] Linda Ross,[1] Ilene Galinsky,[3] Tina N. Davis,[1] Serena J. Silver,[2] David E. Root,[2] Richard M. Stone,[3] Daniel J. DeAngelo,[3] Martin Carroll,[4] William C. Hahn,[2,3] Steven A. Carr,[2] Todd R. Golub,[1,2,5] Andrew L. Kung,[1] and Kimberly Stegmaier[1,2,*]
[1]Department of Pediatric Oncology, Dana-Farber Cancer Institute and Children's Hospital Boston, Harvard Medical School, Boston, MA 02115, USA
[2]The Broad Institute of Harvard University and Massachusetts Institute of Technology, Cambridge, MA 02142, USA
[3]Department of Medical Oncology, Dana-Farber Cancer Institute, Harvard Medical School, Boston, MA 02115, USA
[4]Division of Hematology/Oncology, University of Pennsylvania, Philadelphia, PA 19104, USA
[5]Howard Hughes Medical Institute, Chevy Chase, MD 20815, USA
[6]These authors contributed equally to this work
*Correspondence: kimberly_stegmaier@dfci.harvard.edu
DOI 10.1016/j.ccr.2009.08.018

SUMMARY

Cell-based screening can facilitate the rapid identification of compounds inducing complex cellular phenotypes. Advancing a compound toward the clinic, however, generally requires the identification of precise mechanisms of action. We previously found that epidermal growth factor receptor (EGFR) inhibitors induce acute myeloid leukemia (AML) differentiation via a non-EGFR mechanism. In this report, we integrated proteomic and RNAi-based strategies to identify their off-target, anti-AML mechanism. These orthogonal approaches identified Syk as a target in AML. Genetic and pharmacological inactivation of Syk with a drug in clinical trial for other indications promoted differentiation of AML cells and attenuated leukemia growth in vivo. These results demonstrate the power of integrating diverse chemical, proteomic, and genomic screening approaches to identify therapeutic strategies for cancer.

INTRODUCTION

We previously discovered that epidermal growth factor receptor (EGFR) inhibitors induce acute myeloid leukemia (AML) differentiation and inhibit cell viability with case reports of clinical responses, including two complete remissions (Boehrer et al., 2008; Chan and Pilichowska, 2007; Pitini et al., 2008; Stegmaier et al., 2004, 2005). However, the mechanism by which these molecules induce phenotypic alterations in AML has remained a mystery because EGFR is not expressed in AML (Lindhagen et al., 2008; Stegmaier et al., 2005). This specific example speaks to a more general problem encountered in cell-based, phenotypic screening. Whereas these screens are quite powerful in their ability to identify compounds that modulate complex biological states, the identification of the direct binding target of, or cellular pathway modulated by, a discovered chemical hit can be a serious limitation.

Target identification is critical for the optimization of drug specificity and potency, the minimization of off-target effects, and the monitoring of pharmacodynamic studies in clinical testing. Accordingly, in the absence of a known target, translation of a compound to clinical trial or optimal use of a compound with demonstrated efficacy can be stymied, even for Food and Drug Administration (FDA)-approved drugs. Indeed, there are many compounds for which the mechanism of action is unknown, even when clinical efficacy has been demonstrated. For example, the thalidomide derivative lenalidomide has been approved by the FDA to treat patients with low or intermediate-1 risk myelodysplastic syndrome (MDS) associated with a deletion 5q cytogenetic abnormality (List et al., 2006).

SIGNIFICANCE

Long-term survival for patients with AML remains poor despite dose-intensive chemotherapy regimens. The identification of pharmacologically tractable targets offers an alternative treatment strategy. We build upon our prior observation that multiple EGFR inhibitors possess anti-AML activity via a non-EGFR mechanism. We develop a strategy to identify their off-target activity, integrating proteomic and RNAi-based screening approaches. We identify the kinase Syk as a therapeutic target in AML and demonstrate that a Syk inhibitor has activity in AML cell lines, primary patient blasts, and in vivo AML models. With Syk inhibitors already in Phase II trials, these studies can be immediately translated to the clinic and demonstrate the feasibility of a paradigm for target identification in cell-based screens.

However, the majority of patients with MDS lack the 5q deletion, and, of these patients, a minority respond to lenalidomide (List et al., 2005). Similarly, sorafenib, initially developed as a RAF inhibitor, has been approved for patients with advanced renal cell carcinoma (RCC) in which the relevant target is likely to be a non-RAF tyrosine kinase (Escudier et al., 2007; Ratain et al., 2006). Further optimization in the treatment of RCC ideally would be directed at the relevant target. Because the precise mechanism of action of these drugs is not clear, it has been difficult to identify a priori which patients will benefit from the drug. Similarly, in the absence of target knowledge, our understanding of the development of resistant disease is limited at best.

Although target identification has been a significant roadblock to cell-based screening, this problem now warrants revisiting. With advances such as the application of high-throughput short hairpin RNA (shRNA) screening to mammalian systems and emerging abilities to evaluate the phosphorylated tyrosine kinome, interdisciplinary solutions to this challenge are now feasible. We decided to undertake this challenge of target identification by using integrative orthogonal proteomic and genetic approaches. We explored this strategy in the context of the gene expression-based screen that identified gefitinib as an inducer of AML differentiation (Stegmaier et al., 2004, 2005). As in the case of phenotype-based screening, expression-based screening faces the challenge of identifying the protein target of confirmed compound hits. Here, we integrated immunoaffinity profiling of tyrosine phosphorylation by mass spectrometry and RNAi-based signature screening to identify candidate gefitinib targets and validated one of these kinases as a target for AML therapy.

RESULTS

Proteomic and Genetic Approaches Identify Syk as a Candidate Gefitinib Target

Because multiple EGFR inhibitors induce the AML differentiation phenotype, we hypothesized that a shared off-target kinase was the target in AML differentiation. In order to identify candidate targets, we integrated peptide immunoprecipitation (IP)-HPLC-mass spectrometry and RNAi-based signature screening. Specifically, we employed a proteomics approach that involved IP with a cocktail of three phosphotyrosine antibodies after enzymatic digestion to enrich for phosphotyrosine peptides (Figure S1 available online) (Rush et al., 2005). We treated the AML cell line HL-60 with gefitinib or vehicle for 10 min and then identified peptide phosphorylation sites that were lost after gefitinib treatment by LC-MS/MS (Figure 1A; Table S1). Syk was identified as one of the few tyrosine kinases that exhibited loss of phosphorylation posttreatment. Syk is a nonreceptor tyrosine kinase that was previously shown to play an important role in normal B cell differentiation and hematopoietic signaling and has been implicated in hematological malignancies such as MDS and lymphoma (Chen et al., 2008; Cheng et al., 1995; Chu et al., 1998; Feldman et al., 2008; Kanie et al., 2004; Kuno et al., 2001; Rinaldi et al., 2006; Sada et al., 2001; Turner et al., 1995; Young et al., 2008). Two other direct targets of Syk kinase activity, the adaptor protein Vav1 and the ubiquitin ligase Cbl, were also differentially phosphorylated (Deckert et al., 1996; Lupher et al., 1998).

In order to increase our confidence in hits identified by this proteomics screen, we performed an orthogonal shRNA screen with a lentivirally delivered shRNA library targeting the human kinome (Moffat et al., 2006). We screened 5036 shRNAs for those that induced a complex 19-gene signature of myeloid differentiation (Table S2). Gene expression was measured by the previously described approach: Gene Expression-based High-throughput Screening (GE-HTS) (Stegmaier et al., 2004). GE-HTS is based on the premise that gene expression signatures can be used for high-throughput screening. GE-HTS overcomes some of the challenges inherent in traditional target- and phenotype-based screening in that it is generic, does not require unique assay customization, and does not depend on a priori target knowledge. In brief, mRNAs are captured on 384-well plates coated in oligo-dT and are reverse transcribed to create cDNA. Then, ligation-mediated amplification (LMA) is performed for marker-gene amplification with universal primers (one set biotinylated). Molecular barcodes are incorporated into the flanking regions of each amplicon and are detected by fluorescent beads, each coupled to a capture oligonucleotide complementary to one of the barcodes. The use of beads of different colors (each corresponding to a different barcode capture probe) facilitates quantitation of the LMA products by dual color flow cytometry. Bead color denotes the signature transcript identity, and the phycoerythrin intensity denotes the transcript's abundance (Peck et al., 2006). In this integrative approach to target identification, we combined high-throughput RNAi-based screening with high-complexity signature-based readouts. In the primary RNAi screen, the total hit rate was 2% for shRNAs scoring across all scoring metrics. One of these top-scoring shRNAs targeted *SYK* (Figure 1B). This shRNA suppressed SYK to the most significant degree of the five *SYK*-directed shRNAs included in the screen.

SYK-Directed RNAi Induces Myeloid Differentiation in AML Cell Lines

In a secondary screen performed in two AML cell lines, HL-60 and U937, we tested a collection of additional shRNAs designed to target the top-scoring candidate kinases with an expanded 32-gene myeloid differentiation signature detected by the GE-HTS assay (Table S3). Multiple shRNAs specific for *SYK* scored in both cell lines. We next confirmed that the shRNAs that triggered the 32-gene differentiation signature indeed suppress *SYK* expression (Figures 2A and 2B; Figure S2). These shRNAs also induce morphological evidence of differentiation, including nuclear condensation and cytoplasmic ruffling (Figure 2C), and expression of the mature myeloid cell surface proteins CD11b and CD14 (Figure 2D; Figure S3A). Expression of shRNAs that induced the greatest degree of gene suppression generally resulted in the most striking phenotypic changes. Taken together, these results suggest that loss of Syk in the HL-60 and U937 cell lines induces evidence of AML differentiation by multiple measurements.

Pharmacological Inhibition of Syk Induces Myeloid Differentiation in AML Cell Lines

If Syk plays a role in counteracting differentiation in AML cells, specifically designed pharmacological Syk inhibitors should

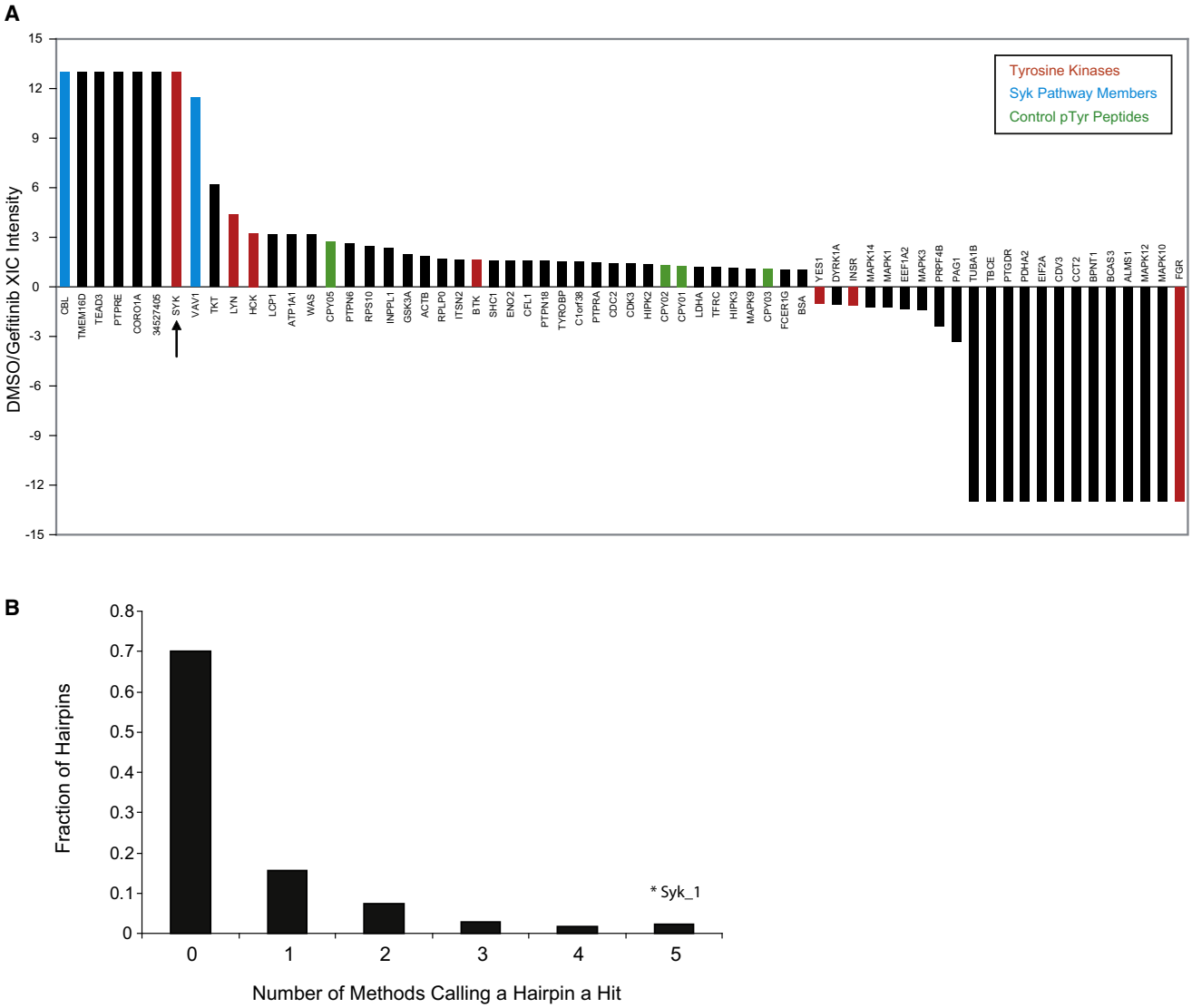

Figure 1. Proteomic and RNAi-Based Approaches Identify Syk as a Target for AML Differentiation

(A) Peptide-IP/LC-MS/MS was used to identify proteins dephosphorylated upon gefitinib treatment. HL-60 cells were treated with vehicle (DMSO) or gefitinib at 10 μM for 10 min. Phosphotyrosine peptides were identified in Syk, Cbl, and Vav1, which were dephosphorylated with gefitinib. The LC-MS/MS extracted ion currents (XIC) for all identified pTyr peptide precursor ions belonging to an individual protein were summed and used to calculate differential expression ratios in DMSO- and gefitinib-treated cells. The specific phosphopeptides and pTyr sites observed are shown in Table S1. CPY01,2,3,5 are control pTyr peptides spiked into each sample at the same concentration. Positive ratios indicate higher expression for DMSO treatment; negative ratios indicate higher expression for gefitinib treatment. Ratios of 13 and −13 indicate that phosphopeptides for a protein were only detected in one of the treatments.

(B) High-throughput RNAi Screen Performance. Five scoring methods were used for identifying hairpins inducing a myeloid differentiation signature (Summed Score, Weighted Summed Score, Naive Bayes, K-Nearest Neighbor, and Support Vector Machine). The majority of shRNAs did not score by any method. The *SYK*-specific shRNA (Syk_1) scored in all methods.

exhibit prodifferentiation activity. To address this hypothesis, we chose to focus on the potent Syk inhibitor already in clinical development, R406, an ATP-competitive pyrimidinediamine with less potency reported for FLT-3, c-Kit, and Lck (Braselmann et al., 2006; Weinblatt et al., 2008). First, we confirmed that treatment with either R406 or gefitinib resulted in inhibition of Syk phosphorylation at Y525/526, the kinase activation site (Figure 3A). As we found when we suppressed *SYK* expression with shRNAs, pharmacological inhibition of Syk induced differentiation in HL-60 and U937 cells, as measured by multiple assays: a 32-gene differentiation signature (Figure 3B); morphological changes, including nuclear condensation and cytoplasmic ruffling (Figure 3C); mature cell surface proteins CD11b and CD14 (Figure 3D; Figure S3B); and nitro-blue tetrazolium reduction (Figure 3E), a functional assay of myeloid maturation measuring superoxide anion production. Taken together, these genetic and pharmacologic studies implicate Syk as a negative regulator of differentiation in AML.

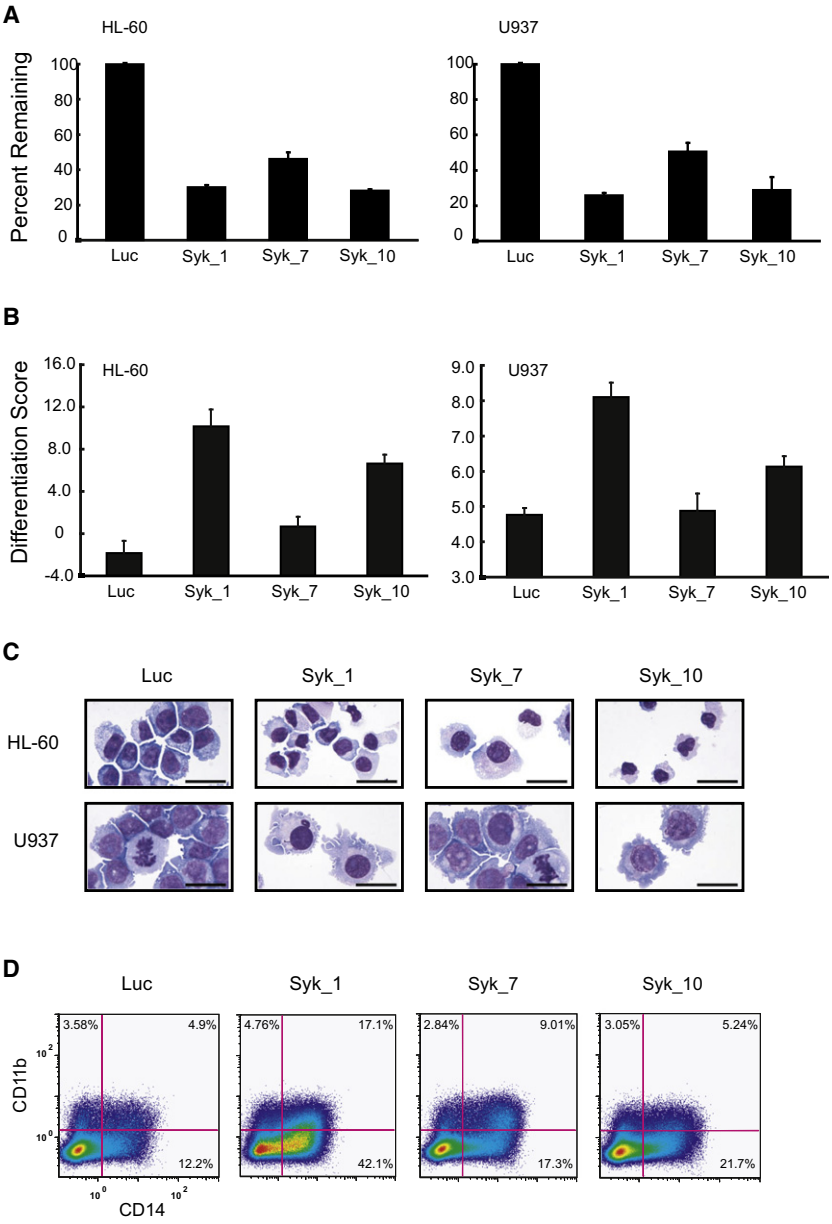

Figure 2. *SYK*-Directed shRNA Induces Differentiation in AML Cell Lines

(A) Knockdown performance of shRNAs targeting *SYK* in HL-60 and U937 cell lines. Transcript levels were measured at 5 days postinfection with real-time PCR and are reported for each hairpin (Syk_1, Syk_7, and Syk_10) relative to the transcript level of a luciferase shRNA control (Luc). Error bars depict mean ± standard deviation (SD) across three replicates.

(B) HL-60 and U937 cells were infected with shRNAs targeting *SYK* and luciferase (Luc), and differentiation was evaluated 7 days postinfection. A 32-gene differentiation signature was quantified by the LMA/bead-based approach, and a weighted summed score (differentiation score) was calculated for all genes. Error bars denote mean ± SD of 16 replicates. The two *SYK*-specific shRNAs that induced the greatest degree of gene suppression also induced the highest differentiation score.

(C) May Grunwald Giemsa staining of HL-60 and U937 cells at 10 and 12 days postinfection, respectively, with shRNAs targeting *SYK* demonstrates cellular differentiation when compared to a luciferase shRNA control. Images were acquired with an Olympus BX41 microscope, 1000× magnification under oil, and Qcapture software. The scale bar represents 25 μm.

(D) FACS analysis was performed with FITC- and PE-labeled antibodies for CD11b and CD14, respectively. At six days postinfection with shRNAs targeting *SYK*, HL-60 cells were positive for single-stained CD11b and CD14 and double staining compared to a luciferase control.

Syk Inhibition Affects a Diverse Set of AML Cell Lines

To determine whether Syk inhibition has broad applicability in AML, we extended testing to additional AML cell lines, evaluating effects of pharmacologic and genetic inhibition on growth and differentiation. When we tested doses up to 10 μM, we found that all of the AML cell lines tested, except for THP-1, exhibited decreased viability (Table S4). We hypothesized that Syk would be differentially phosphorylated across these AML samples, and that phosphorylation status would predict response to Syk inhibition. Consistent with this notion, the two cell lines with the greatest degree of Y525/526 phosphorylation, MOLM-14 and KG-1, were among the most sensitive to the effects of pharmacological inhibition of Syk on viability, apoptosis, and colony formation in methylcellulose (Figures 4A and 4B; Figure S4). In contrast, R406 had minimal effects on apoptosis in HL-60 cells until a dose of 6 μM (data not shown). However, some AML cell lines that exhibited Y525/526 phosphorylation, such as THP-1, were relatively insensitive to R406, whereas Kasumi-1 with lower levels of p-Syk were quite sensitive, suggesting that at least in vitro there are factors other than the degree of Syk phosphorylation that modify response to R406.

We next evaluated the genetic inhibition of Syk in MOLM-14 and KG-1 cells. The introduction of *SYK*-specific shRNA dramatically inhibited the proliferation of these cells (Figure 4C). Ectopic expression of a TEL-Syk cDNA immune to the shRNA rescued the phenotypic alteration, suggesting that the effects of the shRNA were on-target for Syk (Figure 4D). Although both perturbagens induce differentiation in KG-1 cells, as measured by morphological and gene expression changes that precede apoptosis (Figures 4E and 4F; Figure S5), their predominant effects in MOLM-14 cells were on reduced cell viability. However, the subtle effects of the shRNA on differentiation were also rescued with the expression of TEL-Syk. (Figures S6 and S7). These results suggest that the effects of Syk inhibition on differentiation and apoptosis can be uncoupled. Indeed, this uncoupling was previously demonstrated for the EGFR inhibitor erlotinib in AML (Boehrer et al., 2008). Several lines of evidence support the conclusion that the primary consequence of R406 is due to

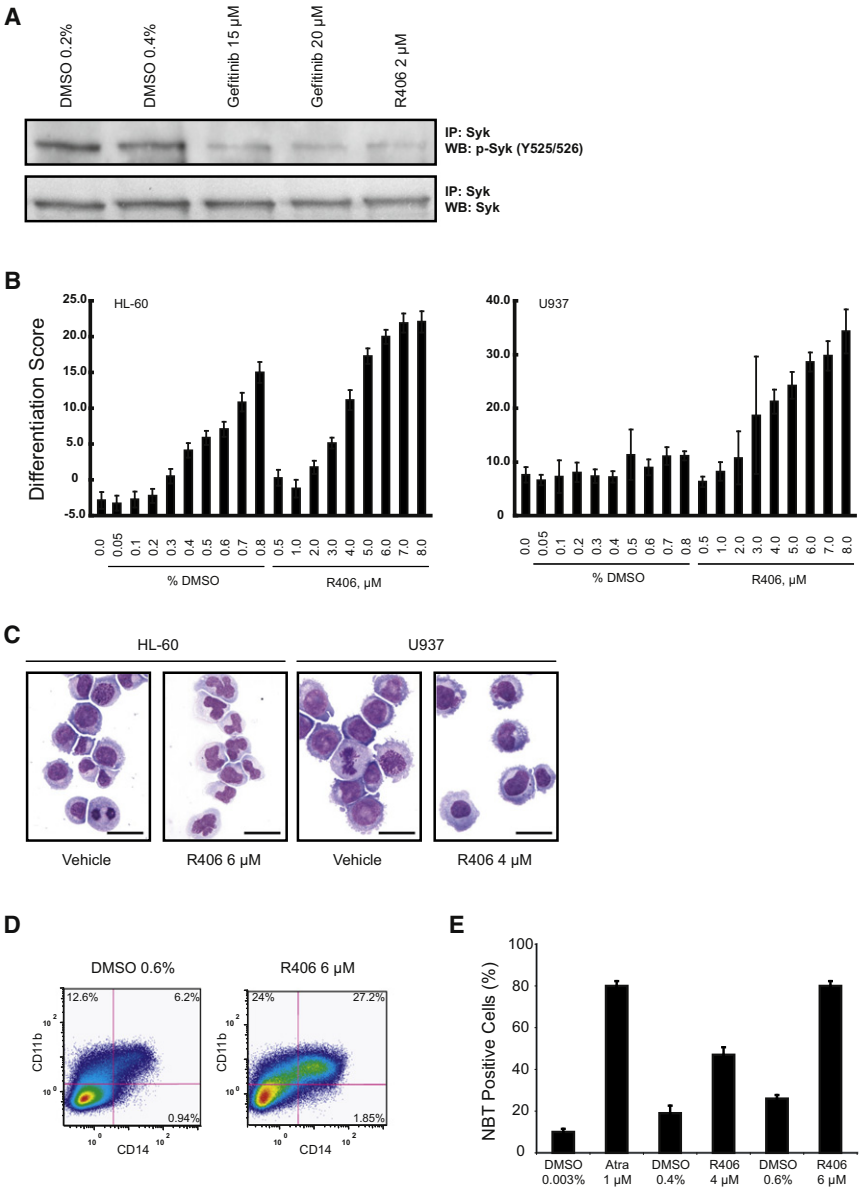

Figure 3. R406 Induces Differentiation in AML Cell Lines

(A) Immunoblot of HL-60 cells treated with vehicle, gefitinib, or R406 for 1 hr. Lysates were immunoprecipitated with anti-Syk antibody and blotted with antibody to p-Syk (Y525/526). Treatment with gefitinib and R406 dephosphorylates Syk at Y525/526. Total Syk was evaluated for a loading control.

(B) HL-60 and U937 cells were treated for 3 days with R406 and DMSO, and a weighted summed score (differentiation score) was determined. Error bars denote the mean ± SD of 16 replicates. A dose response was seen in both cell lines. High-dose DMSO is known to induce differentiation in HL-60; however, the Differentiation Score is higher for each corresponding dose of R406.

(C) May Grunwald Giemsa staining of HL-60 and U937 cells treated for 3 days with DMSO or R406. R406 induces myeloid maturation in both cell lines, as characterized by nuclear condensation and cytoplasmic ruffling. Images were acquired with an Olympus BX41 microscope, 1000× magnification under oil, and Qcapture software. The scale bar represents 25 μm.

(D) FACS analysis was performed with FITC- and PE-labeled antibodies for CD11b and CD14, respectively. HL-60 cells were treated for 3 days with vehicle or R406. R406 induced both CD11b- and CD14-stained double-positive cells and single-stained positive CD11b, consistent with myeloid maturation.

(E) HL-60 cells were treated in triplicate for 3 days with vehicle, ATRA, or R406. The percentage of NBT-positive cells and mean ± SD are shown. Both ATRA and R406 reduced NBT, consistent with the functional maturity of HL-60 cells.

its effects on Syk rather than an off-target kinase of R406. Specifically, we found that *SYK*-specific shRNAs recapitulate the effects of R406. Second, there is a tight correlation between loss of Syk phosphorylation with R406 at Y525/526 and the differentiation score (Figure S8). Moreover, many of the samples that we used harbor wild-type FLT-3, and FLT-3 wild-type cell lines did not respond to a FLT-3 inhibitor (Figure S9).

Pharmacological Inhibition of Syk Has In Vivo Activity in an Orthotopic AML Cell Line and Syngeneic Mouse Models of AML

Although evaluation of human cell lines in vitro is invaluable in the preclinical testing of potential antileukemia compounds, the ex vivo environment cannot fully recapitulate the bone marrow niche. Thus, in vivo studies are critical. Because KG-1 cells had the most dramatic level of Syk phosphorylation, we focused our attention on this cell line. First, we evaluated colony formation in methylcellulose. Both chemical and genetic inhibition of Syk abrogated colony-forming potential in KG-1 cells (Figure 5A; Figure S4). Next, we used an orthotopic xenograft model in which KG-1 cells were labeled with luciferase and propagated in NOD-SCID IL2Rγ^{null} (NOG) xenografts. Eight days of treatment with R788, the prodrug of R406, resulted in significantly decreased leukemia burden ($p < 0.05$) and spleen weight ($p < 0.001$) compared to control-treated animals (Figure 5B; Figure S10). Moreover, to confirm these findings made in human cancer cell lines in primary murine AML, we extended in vivo testing of Syk inhibition to a syngeneic mouse model of MLL-AF9 AML (Stubbs et al., 2008). Again, 8 days of treatment with R788 resulted in significantly decreased leukemia burden ($p < 0.005$) and spleen weight ($p < 0.01$) compared to control-treated animals (Figure 5C; Figure S11).

Syk Is Constitutively Active in Primary AML Blasts

Cell lines have been a critical tool for cancer discovery, but extrapolation of response to primary disease can be problematic secondary to selection for, or acquisition of, additional genetic

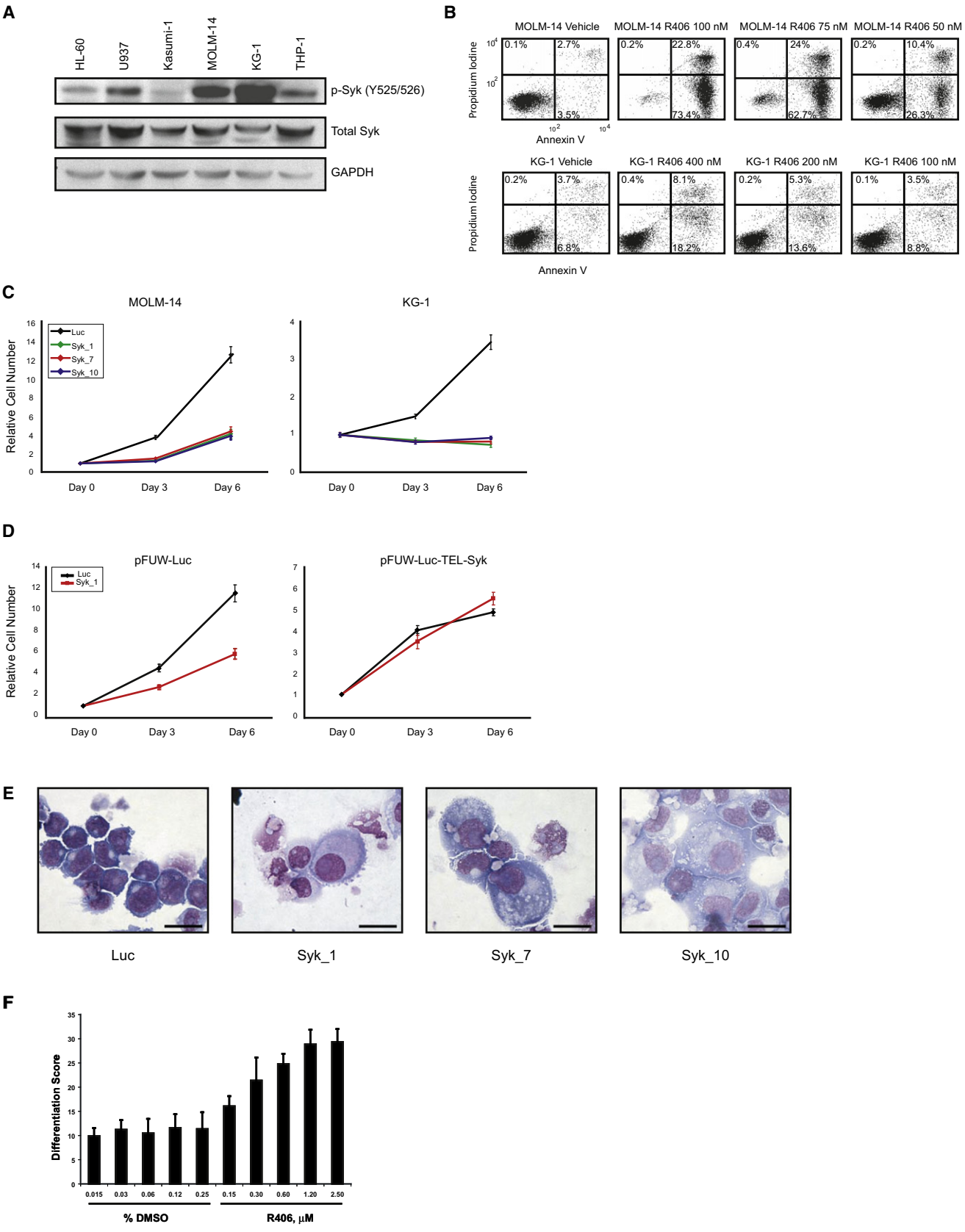
A
HL-60
U937
Kasumi-1
MOLM-14
KG-1
THP-1
p-Syk (Y525/526)
Total Syk
GAPDH
B
MOLM-14 Vehicle
MOLM-14 R406 100 nM
MOLM-14 R406 75 nM
MOLM-14 R406 50 nM
Propidium Iodine
Annexin V
KG-1 Vehicle
KG-1 R406 400 nM
KG-1 R406 200 nM
KG-1 R406 100 nM
C
MOLM-14
KG-1
Relative Cell Number
Luc
Syk_1
Syk_7
Syk_10
Day 0
Day 3
Day 6
D
pFUW-Luc
pFUW-Luc-TEL-Syk
E
Luc
Syk_1
Syk_7
Syk_10
F
Differentiation Score
% DMSO
R406, μM

hits ex vivo. Although studies in primary patient AML blasts are notoriously challenging, they are critical in the validation of therapeutic targets and response to small-molecule inhibitors. We first determined whether Syk is expressed in primary AML blasts. Syk mRNA had previously been reported to be widely expressed in AML (Tomasson et al., 2008), and we identified Syk protein in over 90% of primary AML samples evaluated by immunoblotting (Figure S12). Moreover, using phosphorylation at Y525/526 as a marker of Syk activation, we identified Syk phosphorylation that was abrogated by R406 in an independent collection of primary patient AML blasts for which we obtained adequate cells (Figure 6A). These observations suggested that Syk was not only expressed but constitutively active in primary AML blasts.

The Majority of Primary AML Blasts Respond to Syk Inhibition In Vitro

We next asked whether Syk inhibition would induce differentiation and/or inhibit cell viability in primary AML blasts in vitro. First, we tested the in vitro activity of R406 in primary cells from a patient with acute promyelocytic leukemia (APL), the clinical AML subtype most responsive to differentiation therapy in vivo. Syk inhibition induced differentiation, evaluated by changes in gene expression and morphological appearance with nuclear condensation and lobulation, comparable to the well-validated differentiation agent, all-*trans* retinoic acid (ATRA) (Figure 6B). We next extended testing to 13 additional AML patient samples widely representing the French-American-British (FAB) subclasses and one chronic myelomonocytic leukemia (CMML) sample. Twelve of these thirteen AML patient samples responded with an IC_{50} (drug concentrations that reduced cell viability to 50 percent of the vehicle controls) less than 1 μM at 3 days (range of 0.05 to 0.7 μM) (Figure 6C; Table 1). We noted that one sample from a patient with relapsed M1-AML and another from a patient with CMML failed to respond at doses up to 4 μM. R406 induced evidence of differentiation in 6 of 13 evaluable patient samples in addition to the APL sample (Figures 6B and 6C). As in the case of AML cell lines, the effects of R406 on differentiation and viability were sometimes uncoupled. Treatment response was independent of the FAB subtype.

Pharmacological Inhibition of Syk with R788 Has Activity in a Primary AML Orthotopic Model and a Therapeutic Index in AML

There is an ongoing debate about the utility of conventional mouse models for predicting successful therapies in humans. In response, there has been a shift in the experimental approach to in vivo animal studies; mouse models with tumors collected directly from primary human tumors have been developed. In order to address this issue, we tested R788 in a primary human AML orthotopic model. A primary patient M4-AML sample responsive in vitro to R406 (patient 11) was used for generating a human xenograft in NOG mice by tail vein injection. Seventy days postinjection, mice developed greater than 40% peripheral AML blasts, as measured by human specific $CD45^+$ cells from peripheral blood. Mice were then divided into two cohorts, with two animals per cohort. One group received R788, the second a placebo. A NOG control mouse without human AML was included. Six days posttreatment, tail vein blood was sampled, and the two treated animals were noted to have a decrement in human specific $CD45^+$ cells (Figure 7A). At day 7, animals were sacrificed. Spleen weights were dramatically different across the groups: control mouse, 0.03 g; placebo-treated, 0.14 g and 0.16 g; and R788-treated, 0.04 g and 0.05 g. Histopathology of the bone marrow and spleen (Figure 7B) revealed a dramatic decrease in the number of infiltrating AML cells. We next explored the therapeutic window of R406 by comparing the effects of R406 on primary AML blast colony formation in methylcellulose compared to normal $CD34^+$ myeloid progenitor cells. All six primary AML samples were more sensitive to the effects of R406 than were the normal CD34 myeloid progenitor cells, suggesting that there is a therapeutic index for R406 in AML (Figure 7C).

DISCUSSION

Cure rates for patients with AML have remained poor despite intensive chemotherapy and stem cell transplantation. For older adults, long-term survival is dismal, and many older patients are unable to tolerate standard cytotoxic therapy. Although much has been learned about the pathogenesis of AML, many of the potential targets involve abnormalities of transcription factors, a class of proteins considered "undruggable" with standard pharmacological methods. Emerging approaches, such as RNAi-based methods (Vorhies and Nemunaitis, 2009), gene expression-based methods (Lamb et al., 2006; Stegmaier et al., 2007), stapled peptide technology (Walensky et al., 2004), or other peptide-based methods (Polo et al., 2004) may ultimately enable targeting of this important protein class. Alternatively, the identification of more pharmacologically tractable targets in AML offers a parallel route to therapies for this disease.

Figure 4. Syk Inhibition Affects a Diverse Set of AML Cell Lines

(A) Western immunoblot of AML cell lines reveals MOLM-14 and KG-1 cell lines to be highly phosphorylated at the p-Syk (Y525/526) enzymatic site.

(B) MOLM-14 and KG-1 cells were treated with vehicle or R406 for 6 days. Cells were stained with annexin V-FITC and propidium iodine (PI) and evaluated by flow cytometry. R406 treatment induced increased annexin V-positive cells in a dose-responsive manner, consistent with apoptosis.

(C) MOLM-14 and KG-1 cells were infected with shRNAs targeting *SYK* and luciferase. After 8 days of infection, cell viability was evaluated at days 0, 3, and 6 with an ATP-based assay. Genetic loss of Syk resulted in a dramatic decrease in proliferation. Error bars depict mean ± SD across ratios of six replicate measurements at each time point relative to the six replicate measurements at time zero.

(D) Ectopic expression of TEL-Syk immune to the *SYK*-directed shRNA Syk_1 in MOLM-14 cells rescues the effects of Syk knockdown on cell viability. Cell viability was evaluated 4 days after infection at days 0, 3, and 6 with an ATP-based assay. Error bars depict mean ± SD across ratios of eight replicate measurements at each time point relative to the eight replicates at time zero.

(E) May Grunwald Giemsa staining of KG-1 cells at 12 days postinfection with shRNAs targeting *SYK* versus a luciferase shRNA control demonstrates evidence of macrophage-like differentiation. Images were acquired with an Olympus BX41 microscope, 1000× magnification under oil, and Qcapture software. The scale bar represents 25 μm.

(F) KG-1 cells were treated with R406 versus DMSO, and the 32-gene differentiation signature was measured at 24 hr. R406 induces a myeloid differentiation signature, as measured by a weighted summed score (differentiation score). Error bars depict mean ± SD across eight replicates.

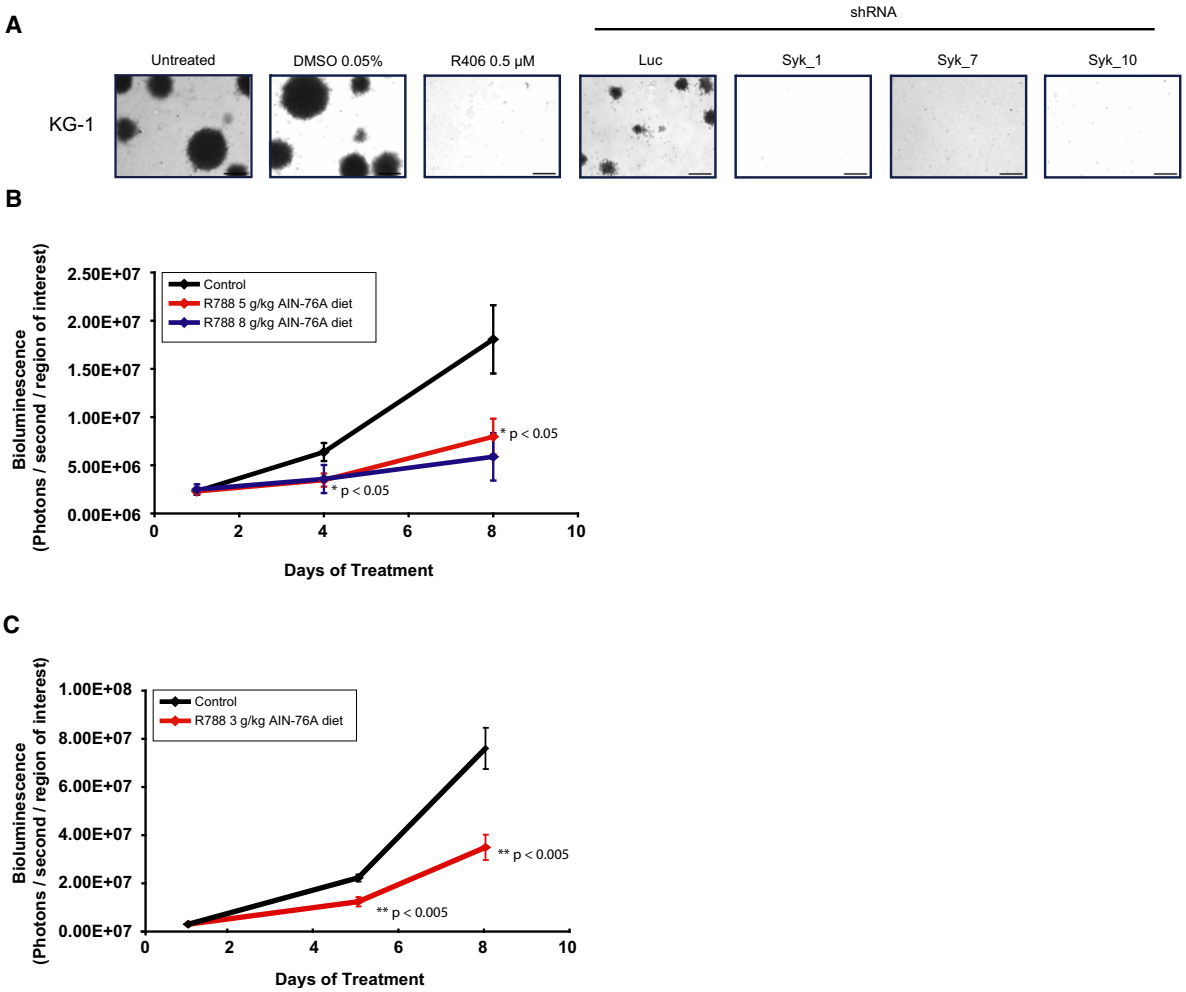

Figure 5. R406 Has In Vivo Activity in AML

(A) The ability of KG-1 to form colonies in methylcellulose with R406 and multiple shRNAs directed against *SYK* was assessed. Both chemical and genetic inhibition of Syk abrogate colony formation in KG-1. The scale bar represents 1 mm.

(B) KG-1 luciferase-positive xenografts were established in NOG mice. Mice were treated with placebo (n = 4), food impregnated with 5 g R788/kg AIN-76A food (n = 5), and food impregnated with 8g/kg AIN-76A food (n = 3) for 8 days. Mice treated with R788 had a significant difference in tumor burden compared to those treated with placebo. Serial in vivo BLI was used to assess disease burden, and data were plotted as the mean ± SEM for each group. One way ANOVA analysis with Tukey post-test was used to determine the significance of all pairwise comparisons.

(C) A syngeneic, luciferase-positive mouse model of MLL-AF9 AML was established in C57BL/6:Tyr$^{C/C}$ mice. Mice were treated with placebo (n = 10) or food impregnated with 3g R788/kg AIN-76 food (n = 10) for 8 days. Serial in vivo BLI was used to assess disease burden and plotted as mean ± SEM. Statistical significance was calculated with a Student's t test.

In this work, we build upon the striking observation that multiple EGFR inhibitors had anti-AML activity via a non-EGFR mechanism, and we hypothesized that this was via a shared off-target effect. We integrate cross-disciplinary proteomic and genetic approaches to meet the difficult challenge of understanding the molecular basis for the biological activity of these EGFR inhibitors in AML. At the intersection of these two approaches, Syk was identified as a tyrosine kinase target in AML. Syk is a cytoplasmic tyrosine kinase widely expressed in hematopoietic cells and critical in B cell differentiation and signal transduction pathways. Syk is a member of the Syk/ZAP-70 family of nonreceptor kinases and is characterized by two N-terminal Src homology 2 domains and a C-terminal kinase domain separated by a flexible linker (Sada et al., 2001). Syk activation has been implicated in a variety of hematopoietic cellular responses (Chu et al., 1998; Sada et al., 2001; Turner et al., 2000), and there is a growing literature supporting the role of Syk in hematological malignancies, particularly the lymphomas (Chen et al., 2008; Feldman et al., 2008; Rinaldi et al., 2006; Streubel et al., 2006). Interestingly, we see variable patterns of p-Syk expression and response to R406 in acute lymphoid leukemia cell lines (Figure S13; Table S5).

Our demonstration of a role for Syk in the pathogenesis of myeloid malignancies is supported by the case report of the fusion of the *TEL* to the *Syk* gene in a patient with MDS with t(9;12)(q22;p12) (Kuno et al., 2001). Importantly, this TEL-Syk fusion transformed the interleukin-3-dependent murine hematopoietic cell line Ba/F3 to growth factor independence (Kanie

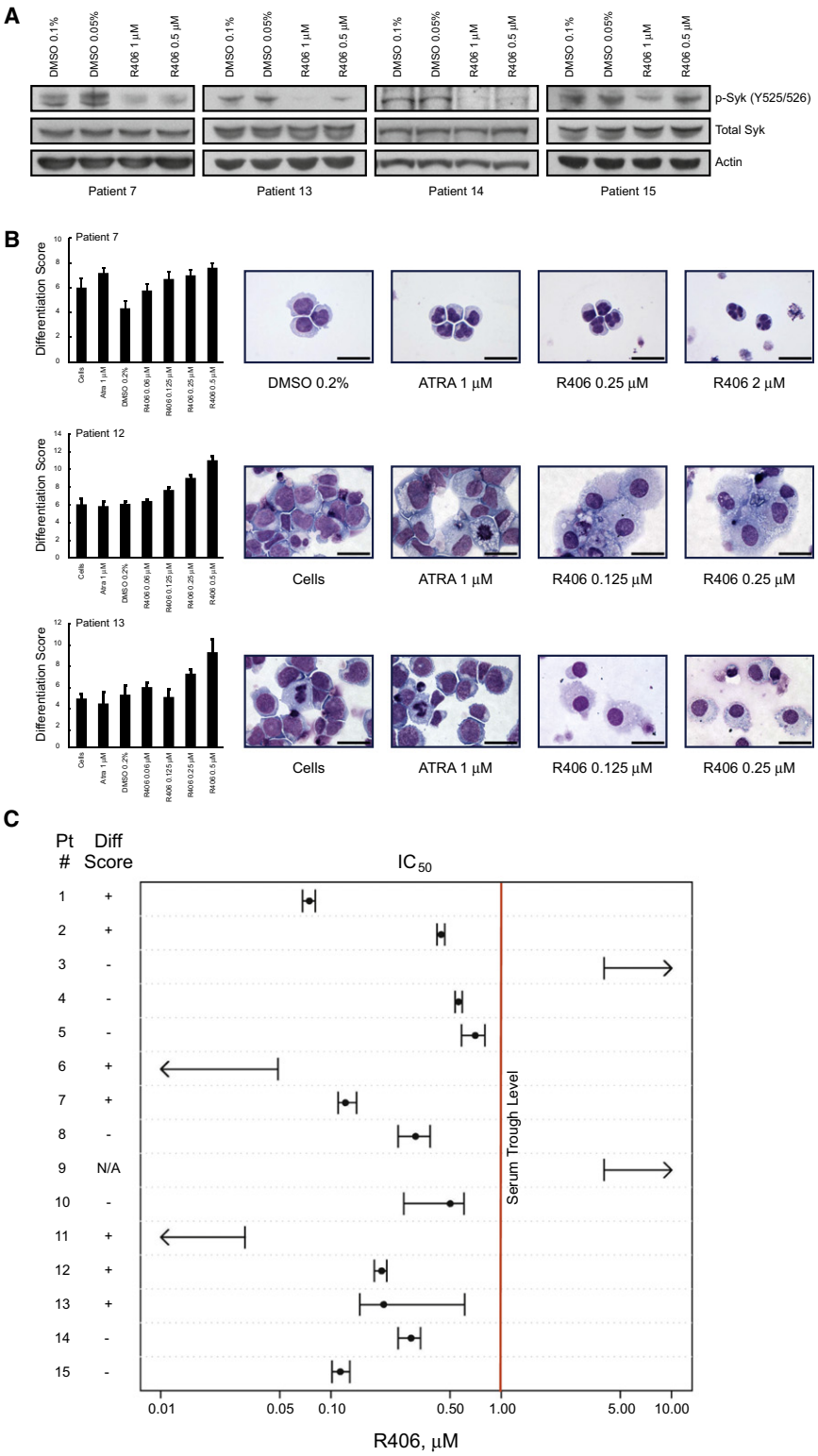

Figure 6. Primary AML Cells Are Responsive to Syk Inhibition In Vitro

(A) Fresh primary patient AML cells were treated in vitro with vehicle versus R406, and Syk phosphorylation at Y525/526 was assessed by immunoblotting. In all four samples, Syk is phosphorylated at the kinase activity site, and this phosphorylation is inhibited by R406.

(B) Primary AML blasts were treated with DMSO, ATRA, or R406 for 3 days, and the 32-gene differentiation signature was evaluated. Error bars denote mean ± SD across eight replicates per condition. R406 induces comparable or greater levels of differentiation to ATRA. May Grunwald Giemsa staining of ATRA- and R406-treated primary AML at 4 days reveals myeloid differentiation with lobulation of nuclei in the APL sample and macrophage-like differentiation in Patients 12 and 13. Images were acquired with an Olympus BX41 microscope, 1000× magnification under oil, and Qcapture software. The scale bar represents 25 μm.

(C) Primary patient AML cells were treated in quadruplicate with R406 in a two-fold dilution series. At day 3, cell viability was evaluated with an ATP-based assay. Values for the IC_{50} are depicted with error bars denoting the 95% confidence interval for the SEM for the four chemical replicates relative to the four control replicates. At day 3, the 32-gene differentiation signature was measured. Samples are scored as differentiating if there was a 1.5-fold change in the Differentiation Score across at least two doses with $p < 0.05$ by a one-tailed t test assuming two samples with unequal variance.

et al., 2004). Syk mRNA transcript has been reported to be expressed in primary AML blasts (Tomasson et al., 2008), and its expression correlated with response to treatment with gemtuzumab ozogamicin (Balaian and Ball, 2006). In our studies, we demonstrate that Syk protein is not only expressed but is also constitutively activated in nearly all of the samples evaluated. Determining the mechanism of activation of Syk and its critical downstream effectors in AML is under active investigation.

The screening of libraries enriched for FDA-approved compounds is an attractive strategy by which to repurpose drugs for alternative indications and to more rapidly test clinically relevant hypotheses in patients. However, the potency and selectivity of such drugs are often not optimal for discovered indications. Moreover, there is the desire to optimize on-target activity and minimize off-target side effects. Although EGFR inhibitors have had anti-AML effects, including complete responses, these molecules do not potently inhibit Syk and are often not well tolerated at doses anticipated to inhibit Syk in vivo. Therefore, we need to identify more potent and selective Syk inhibitors for this indication. The Syk inhibitor R788 is the orally available prodrug of R406. Phase I testing of R788 has been

Table 1. Primary Patient AML Characteristics

Patient	Diagnosis	Cytogenetic Findings	FLT-3 ITD	FLT-3 D835 Codon Change
1	M1-AML	89-92, XXXX	No	No
2	M2-AML	45 XY, -7, inv(3)(q21q26)	No	No
3	CMML	Complex karyotype[a]	N/A	N/A
4	M4-AML	46 XY	No	D835H
5	M4-AML	46 XX	No	D835E
6	M2-AML	46 XX	Yes	No
7	M3-AML	47 XX, +8, t(15;17) (q22;q21)	Yes	No
8	M4-Eo	45 X,-Y[11]/46, XY[9]. Nuc ish (CBF x2) [100]	No	No
9	M1-AML	46 XX	No	No
10	M-5b-AML	46 XX	No	D835Y
11	M4-AML	46 XY	Yes	No
12	AML[b]	N/A	Yes	No
13	AML[b]	46 XY	No	No
14	M4-AML	46 XY	Yes	No
15	AML[b]	47 XX, +8 [19]/46, XX [1]	Yes	No
31	M7-AML	52,XY,+8,+14,+19,+21,+21, +21c[14]/47,XY,+21c[6]	N/A	N/A

N/A, not available.
[a] 46, XY, t (1;19) (p36;q13), del (2) (p2?3), t (3;15) (p21;q22), add (4) (q35), -6, der (7) t (7;14) (q36;q11.2), -14, -21 + mar [cp10]/46 XY, del (2) (p2?1), add (7) (q11.2) [cp4]/46, XY, add (1) (q42), t (1;14) (p12;q11), del (3) (q1?3), der (7) del (7) (q3?1q3?4) t(3;7) (q13;p22, t(17;21) (q2?1;q22) [2]/46, XY, nonclonal abnormalities [4].
[b] FAB not reported.

completed with peak concentrations in excess of 10 μM, steady-state concentrations of 1–3 μM, and trough concentrations of 1 μM (E. Grossbard and Rigel Pharmaceuticals, personal communication). In phase I testing in patients with rheumatoid arthritis and heavily pretreated patients with lymphoma, the drug has been well tolerated, and significant clinical activity has been demonstrated (Weinblatt et al., 2008; M. Shipp, personal communication). In our studies, the majority of primary patient AML samples responded in a clinically achievable dose range, with an IC_{50} below the serum trough concentration in humans. Thus, these observations suggest that inhibition of Syk can be achieved with doses in use in current clinical trials.

The last decade has seen a marked shift in the approach to cancer-related small-molecule library screening performed by the pharmaceutical industry with a transition away from phenotype-based screening and a primary focus now on target-based screening. Although target-based screening has been successful for known, tractable protein targets, as with any approach, it does have limitations. The majority of known oncoproteins are not considered easily druggable, and for many malignancies, driver events have not yet been identified. In addition, target-based screening is most commonly performed with ex cellulo assays and may not fully recapitulate the complexity within a cell. Alternative screening approaches, such as traditional phenotype-based and expression-based approaches, create the possibility of screening in the absence of a priori target knowledge. Moreover, expression-based screening holds promise for modulating intractable targets and can be systematized as a screening paradigm. However, the transition from compound discovery to drug development has been stymied for these cell-based screens by the challenge of identifying the protein target of the identified compound. Emerging genomic, genetic, and proteomic approaches have altered the landscape of target identification for cancer. Similarly, these approaches can transform the drug discovery process. Their integration into the compound discovery phase has already begun. Our work suggests that a cross-disciplinary integration of genome-wide expression profiling, proteomics, and high-throughput RNAi-based screening could systematize protein target identification for cell-based chemical screens. Moreover, innovations in synthetic chemistry and proteomics should further facilitate this process in the future. For example, diversity-oriented synthesis of small-molecule collections allows for the incorporation of chemical handles to facilitate efficient, systematic attachment of affinity resins (Burke et al., 2003). After affinity capture, the specific protein/compound interactions can be identified by differential isotopic labeling of amino acids as recently described (Ong et al., 2009).

In conclusion, we demonstrate that the majority of AML cell lines and primary blasts, and three in vivo AML models, had a therapeutic response to Syk inhibition with effects on cell growth and differentiation. With an orally available, well-tolerated Syk inhibitor currently in clinical development for other indications, the results reported here should have immediate relevance for clinical testing of Syk inhibition in patients with AML. Furthermore, these results demonstrate the feasibility of integrating shRNA-based screening and phosphoproteomic studies to identify small molecules and their mechanisms of action.

EXPERIMENTAL PROCEDURES

Cell Culture

Primary patient AML blasts were collected from peripheral blood or bone marrow aspirate after obtaining patient informed consent under Dana-Farber Cancer Institute- and the University of Pennsylvania Internal Review Board-approved protocols. Mononuclear cells were isolated with Ficoll-Paque Plus (Amersham Biosciences), and red blood cells were lysed. Cryopreserved human bone marrow $CD34^+$ cells were obtained from Poietics, and use of these materials is considered exempt as human subjects by the Dana-Farber Cancer Institute Internal Review Board.

HL-60, U937, Kasumi-1, and KG-1 were purchased from the American Type Culture Collection. THP-1, MOLM-14, 697, NALM-6, REH, RS4-11, SEMK2, and SUP-B15 were kindly provided by Dr. Scott Armstrong. DND-41, HPBALL, KOPTK1, MOLT-4, and PF-382 were all kindly provided by Dr. Jon Aster. All cell lines and primary patient cells were maintained in RPMI 1640 (Cellgro) supplemented with 1% penicillin-streptomycin and 10% fetal bovine serum (Sigma-Aldrich) at 37°C with 5% CO_2.

Chemicals

Gefitinib (WuXi PharmaTech, Shanghai, China) and all-*trans* retinoic acid (ATRA) (Sigma-Aldrich) were dissolved in dimethyl sulfoxide (DMSO) and stored at −20°C. R406 (Rigel Pharmaceuticals, Inc., San Francisco, CA) was resuspended in DMSO and stored at −80°C. R788 was also supplied by Rigel Pharmaceuticals.

Phosphoproteomic Studies

HL-60 cells (1×10^9) were treated in duplicate with 10 μM gefitinib for 10 min. On the basis of a protocol described by Rush et al. (2005), protein lysate was extracted with a urea-containing lysis buffer and protease inhibitor. Upon reduction of the disulfide bonds and the alkylation of cysteines with

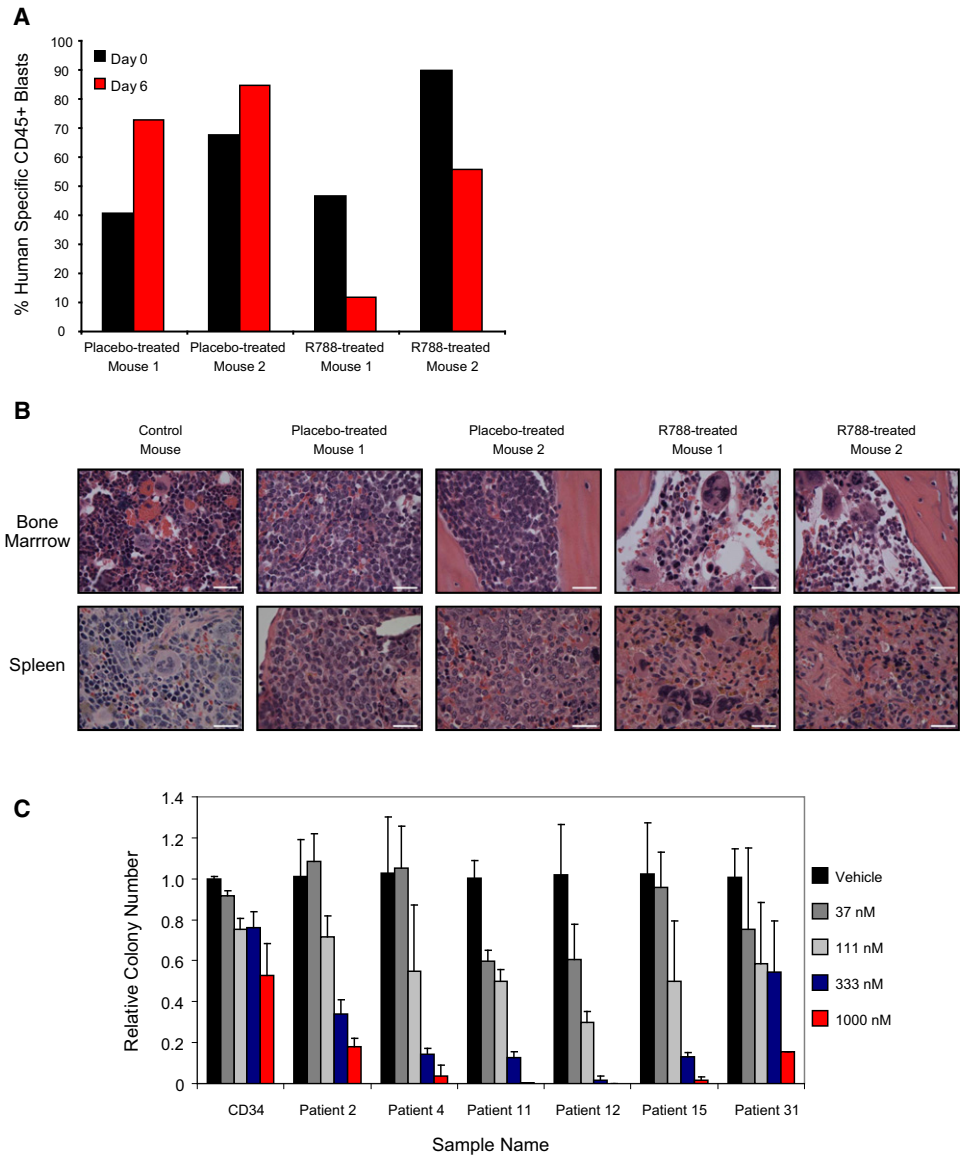

Figure 7. Primary AML Is Responsive to Syk Inhibition in an Orthotopic Model

(A) A primary AML (patient 11) orthotopic xenograft was established in NOG mice. Six days after initiation of treatment with food containing 5g R788/kg AIN-76 rodent diet, the AML blast percentage, measured by percentage of human specific $CD45^+$ cells in peripheral blood, continued to increase in the placebo-treated mice but decreased in the R788-treated mice.

(B) Histopathology studies of bone marrow in R788-treated versus placebo-treated animals reveal near resolution of AML infiltration with areas of necrosis and areas of recovering marrow identified. Hematoxylin and eosin staining of spleen reveals areas of leukemic infiltration and extramedullary hematopoiesis in placebo-treated mice and near resolution of AML infiltration in the R788-treated animals. Images were acquired with an Olympus BX41 microscope, 1000× magnification under oil, and Qcapture software. The scale bar represents 25 μm.

(C) The ability of normal CD34 myeloid progenitor cells and primary patient AML blasts to form colonies in methylcellulose with R406 was assessed. Colony formation was assessed in duplicate, and colonies per 4 cm^2 were counted and displayed relative to control cells. Error bars depict mean ± SD across four ratios of dose response to vehicle. Primary patient AML blasts were more sensitive to the effects of R406 than were normal myeloid progenitors.

iodoacetamide, the lysate was split into two aliquots and diluted with 20 mM HEPES to 2 M or 0.5 M urea before digestion with trypsin or chymotrypsin, respectively. The total peptide mixtures were then desalted by Sep-Pak cartridge and resuspended in immunoprecipitation (IP) buffer, 50 mM MOPS/NaOH (pH 7.2), 10 mM Na_2PO4, 50 mM NaCl, along with four exogenous pTyr-containing peptides added as controls. IP was performed with a cocktail of three protein G agarose bead-bound phosphotyrosine antibodies, pY100 (Cell Signaling), 4G10 (UpState), and pY99 (Santa Cruz Biotechnology), to enrich for phosphotyrosine-containing peptides. Peptides captured by phosphotyrosine antibodies were eluted under basic solutions and then under acidic conditions. The IP eluates were analyzed by data-dependent LC/MS/MS with a ThermoFisher LTQ-Orbitrap instrument. All MS and MS/MS data were processed with the Spectrum Mill software package, which assigns peptide identity with a <1% false discovery rate with a target-decoy database search approach, maps phosphorylation sites, and quantitates with extracted ion chromatograms of each peptide precursor ion (Table S1).

Differentiation Studies

Morphological Evaluation

Changes in cellular morphology were evaluated by May Grunwald Giemsa staining (Sigma) under light microscopy under oil at 1000× magnification with an Olympus BX41 microscope and Q-capture software.

Nitro-Blue Tetrazolium Reduction Assay

Nitro-blue tetrazolium (NBT) reduction assays were performed in triplicate. Compound-treated cells were compared to DMSO-treated controls after 3 days of treatment. Cells were incubated at 37°C for 1 hr in a mixture containing total medium, 0.1% NBT (Sigma), and 1 μg/ml TPA (12-*O*-tetradecanoylphorbol-13-acetate; Sigma). The percentage of blue cells was counted by light microscopy for at least 200 cells per sample. Drug-treated cells were compared with DMSO-treated cells with a one-tailed t test analysis assuming two samples with unequal variance.

Flow Cytometry

Cells were stained with 1:25 CD11b-FITC (Beckman Coulter IM0530U) and 1:25 CD14-PE (Beckman Coulter IM0650U) for 30 min and detected by flow cytometry (Beckman Cytomics FC500). Data were analyzed with the FlowJo software package (Tree Star). Fluorescence gating was set based on single-stained mouse Ig κ compensation bead fluorescence intensity (BD Biosciences #552843).

Gene Expression Studies

Marker genes for myeloid differentiation were chosen with previously published Affymetrix AML-related data sets (Stegmaier et al., 2004). We selected an initial collection of 19 genes used in the RNAi primary screen and then an expanded group of 32 genes. (Tables S2 and S3). These genes distinguish AML from either neutrophil or monocyte with $p < 0.05$ by t test and distinguish undifferentiated versus differentiated HL-60 with ATRA, PMA, or VitD with $p < 0.05$ by t test. The GE-HTS assay was performed as detailed in the Supplemental Experimental Procedures. Two primary methods are used to compare signature gene induction. The Summed Score combines expression ratios (marker gene/control gene) by summing them with a sign determined by the expected direction of regulation from gefitinib- or ATRA-treated positive controls. The Weighted Summed Score combines expression ratios by summing them with a weight and sign determined by the signal-to-noise ratio of each expression ratio for the positive control (gefitinib- or ATRA-treated) and negative control (DMSO-treated) samples.

Viability Assay

Viability experiments were performed with the Promega Cell-Titer Glo ATP-based assay per the manufacturer's instructions. Values for IC_{50} (drug concentrations that reduced cell viability to 50 percent of the vehicle controls) were calculated by interpolating a natural cubic spline fit to the measured viability data in R (with the spline function).

Apoptosis Studies

AML cell lines were treated in triplicate with DMSO versus R406 for 6 days. Annexin V FITC/PI staining was performed with the Annexin V:FITC Apoptosis Detection Kit I (BD PharMingen). Cells were analyzed by flow cytometry with a FACScan flow cytometer (Becton Dickinson) and CELLQuest analytical software.

Methylcellulose Colony-Forming Assay

For the RNAi studies, KG-1 and MOLM-14 cells were infected with shRNA directed against a luciferase control or *SYK* (three unique constructs). After 48 hr of puromycin selection, cells were recounted by trypan blue exclusion, and 3×10^4 were plated at 1:10 (vol/vol) in methylcellulose (ClonaCell-TCS Medium, 03814) with 1% penicillin-streptomycin and appropriate drug treatment. For pharmacological treatment of primary AML, AML cell lines, and normal CD34 myeloid progenitor studies, cells were treated with R406 or matched vehicle control for 48 hr in liquid culture. After 48 hr, an equal number of cells were plated at 1:10 (vol/vol) in MethoCult GF+H4435 methylcellulose (StemCell Technologies, #04445) with 1% penicillin-streptomycin and appropriate drug treatment. All plates were incubated at 37°C and 5% CO_2, and colony numbers were counted 8–17 days later.

RNAi Screening

High-throughput screening was performed with the RNAi Platform at the Broad Institute. HL-60 cells were plated in a 384-well format in 30 μl medium at 15,000 cells/well and incubated overnight at 37°C with 5% CO_2. Polybrene (Sigma) was added to a final concentration of 8 μg/ml. The lentivirally delivered sublibrary of the RNAi Consortium shRNA library (http://www.broad.mit.edu/rnai/trc/lib) was screened in quadruplicate (Moffat et al., 2006). Virus was added at 2.5 μl per well, and plates were spun for 30 min at 2250 rpm and were incubated for 48 hr. Selection was performed on three replicates with 1 μg/ml puromycin (Sigma), and medium was changed on the unselected control plate. Uninfected controls included cells only (8 wells), 1 μM ATRA (8 wells), and 25 μM gefitinib (8 wells). Plates were incubated for 72 hr. ATP-based viability was assessed for one puromycin-treated plate and the unselected plate with Cell-Titer Glo (Promega). GE-HTS was carried out on two replicates, as previously described, with a 19-gene myeloid differentiation signature. (see Supplemental Experimental Procedures and Table S2) (Peck et al., 2006; Stegmaier et al., 2004).

Screen plates were filtered and scaled, and five scoring algorithms were applied: Summed Score, Weighted Summed Score, Naive Bayes, K-Nearest Neighbor (KNN), and Support Vector Machine (SVM). An shRNA was considered a hit if the shRNA was classified as being more like gefitinib-treated controls than untreated HL-60 controls by all five methods (see Supplemental Experimental Procedures for details of the analysis). A secondary screen was performed as described above, with the following exceptions: HL-60 and U937 cells were plated at 15,000 cells/well and 4,500 cells/well, respectively. shRNAs that scored in the primary screen, as well as additional available shRNAs developed against the hits, were screened in five replicates. In addition, an expanded 32-gene myeloid differentiation signature was measured (Table S3).

Lentiviral Vectors and Infection

Oligonucleotides encoding shRNAs were cloned into pLKO.1 as described previously (Moffat et al., 2006). Sequences targeted by each *SYK* shRNA are listed in Table S6. For large-scale infections, 500,000 293T cells were plated in 6 cm plates and transfected 24 hr later with 1 μg DNA from lentiviral backbone vector and packaging plasmids (pCMVdeltaR8.91 and pMD.G) according to FuGENE 6 (Roche) protocol. Medium was changed to RPMI 1640 24 hr posttransfection, and viral supernatant was harvested and filtered 48 hr posttransfection. Cells were infected for 2 hr at 37°C with 2 ml lentivirus and 8 μg/ml polybrene (Sigma). Cells were selected 48 hr later with 1 μg/ml puromycin (Sigma).

For generating the TEL-Syk construct, RT-PCR was used to isolate the sequences encoding amino acids 1–336 of human ETV6 (TEL) and amino acids 266–635 of human Syk. The assembled cDNA was subcloned in place of mCherry in the lentiviral plasmid FUW-Luc-mCherry-puro (Kimbrel et al., 2009) to give the plasmid FUW-Luc-TEL-SYK-puro. VSVG-pseudotyped virus was produced by cotransfection of 293T cells along with the helper plasmids delta8.9 and CMV-VSVG. Infection of MOLM-14 was performed as described above.

Real-Time PCR

Total RNA was isolated with TRIZOL reagent (Invitrogen), cDNA was synthesized with SuperScript III Reverse Transcriptase (Invitrogen) and oligo $d(T)_{16}$ primers, and cDNA was analyzed in the real-time quantitative PCR reactions prepared with TaqMan Universal Master Mix (Applied Biosystems). RPL13A expression was evaluated for each sample as a control for total RNA. Primers and probes for real-time RT-PCR were obtained from Applied Biosystems (RPL13A # Hs01926559_g1 and SYK Hs00895374_m1).

Immunoblotting

Cells were lysed in Cell Signaling Lysis Buffer (Cell Signaling) containing Complete, EDTA-free Protease Inhibitor Cocktail Tablet (Roche Diagnostics) and PhosSTOP Phosphatase Inhibitor Tablet (Roche Diagnostics), resolved by gel electrophoresis, and transferred to nitrocellulose membranes (BioRad Laboratories). Blots were incubated with primary antibodies to p-Syk (Y525/526) (Cell Signaling, 2711), total Syk (Santa Cruz Biotechnology, SC-1240), β-Actin (Abcam, ab8227-50), GAPDH (Abcam, ab22556-100), or Vinculin (Abcam, ab18058), followed by secondary antibodies anti-rabbit-HRP (Amersham #NA9340V) or anti-mouse-HRP (Amersham #NA9310V). Bound antibody was detected by chemiluminescence. For IP, 2 mg of each protein in lysis buffer was incubated with 2 μg/ml anti-Syk antibody (Santa Cruz, SC-1240) for

4 hr at 4°C. The immunocomplex was precipitated with 30 μl UltraLink Immobilized Protein A/G beads (Pierce) overnight at 4°C. The beads were then washed twice with cold 1× Cell Signaling Lysis Buffer (Cell Signaling) containing protease inhibitor, resuspended in 10 μl 4× SDS sample buffer, and boiled for 5 min. The protein was then separated by gel electrophoresis and transferred to a nitrocellulose membrane (BioRad Laboratories). Blots were probed with anti-pSyk (Y525/526) (Cell Signaling #2711) and incubated with anti-rabbit-HRP (Amersham #NA9340V). Bound antibody was detected by SuperSignal West Dura Extended Duration Substrate (Pierce).

In Vivo Studies

All animal studies were performed on Dana-Farber Cancer Institute Institutional Animal Care and Use Committee (IACUC)-approved protocols. For KG-1 xenografts, 3 hr prior to injection, 6-week-old male NOD-SCID IL2Rγ^{null} mice (NOG, Jackson Laboratory) were sublethally irradiated with 200 rads. A total of 2 × 10^6 KG-1-LucNeo cells were injected via tail vein, and total body leukemia burden was assessed by bioluminescence imaging (BLI) as previously described (Armstrong et al., 2003). Animals were imaged 5 and 7 days after injection, and mice with established disease were divided into cohorts that were treated with normal feed or feed impregnated with R788 at 5 g/kg or 8 g/kg AIN-76A rodent diet. Serial imaging was used to assess disease burden, and data were plotted as the mean ± standard error of the mean (SEM) for each group. After 8 days on treatment, all mice were euthanized, and tissue was collected. Spleen weights were expressed as mean ± SEM. One way ANOVA analysis with Tukey post-test was used to determine the significance of all pairwise comparisons.

Murine AML was induced by retroviral transduction of bone marrow with MLL-AF9 as previously described (Stubbs et al., 2008). In brief, bone marrow was harvested from a transgenic mouse with ubiquitous luciferase expression (C57BL/6:UbC6-Luc) and transduced with a retrovirus encoding MLL-AF9 (MSCV-MLL-AF9-pgkNeo). Development of leukemia was determined by BLI and clinical scoring. Thirty albino coisogenic mice (C57BL/6:Tyr$^{C/C}$, Jackson Labs) were sublethally irradiated with 300 rads, then injected with 10^6 mononuclear cells isolated from the spleen of a mouse with primary AML. Mice underwent BLI weekly, and at 3 weeks postinjection, animals with documented disease (increasing bioluminescence) were divided into two cohorts of mice with equal mean bioluminescence. The treatment group (n = 10) was started on sdiet impregnated with R788 at 3 g/kg AIN-76A rodent diet. The control group (n = 10) was kept on a normal diet. Mice underwent serial BLI at the indicated days of treatment and were euthanized after the last imaging time point, and tissue was collected. Total body bioluminescence was quantitated with standardized regions of interest (Living Images, Caliper Life Sciences) and are expressed as mean ± SEM. Statistical significance for BLI data and spleen weights were calculated with Student's t test.

For the primary human orthotopic model of AML, NOG mice were sublethally irradiated with 200 rads and then injected by tail vein injection with 4 × 10^5 viable AML cells (Patient 11). Seventy days postinjection, mice developed greater than 40% peripheral AML blasts, as measured by FACS analysis of human specific CD45$^+$ cells from peripheral blood. Mice were then divided into two cohorts, with two animals per cohort. One group received 5g R788/kg AIN-76 rodent diet, and the second, a placebo food. A NOG control mouse without human AML was included. Six days posttreatment, tail vein blood was sampled and peripheral AML blasts were again measured by FACS analysis of human specific CD45$^+$ cells. At day 7, animals were euthanized and tissue was collected.

See Supplemental Experimental Procedures for the full details of experimental methods.

Microarray Data

Previously published raw microarray data (Stegmaier et al., 2004) are available at http://www.broad.mit.edu/cancer/pub/GE-HTS_leuk or http://www.ncbi.nlm.nih.gov/geo.

SUPPLEMENTAL DATA

Supplemental Data include Supplemental Experimental Procedures, 13 figures, and 6 tables and can be found with this article online at http://www.cell.com/cancer-cell/supplemental/S1535-6108(09)00291-8.

ACKNOWLEDGMENTS

We thank Rigel Pharmaceuticals, particularly Elliott Grossbard and Polly Pine, for supplying R406 and R788 chow. We also thank Jen Grenier for RNAi screening guidance; John Daley, Jill Angelosanto, and Kathleen Brosnahan for FACS assistance; Jinyan Du and Shao-En Ong for insight regarding the proteomics experiment; Susan Buchanan for primary sample collection; Jeff Kutock for pathology slide review; Anu Narla and Benjamin Ebert for facilitating testing of normal myeloid progenitor cells; Giovanni Roti, Dorhyun Johng, and Robin Perry for technical assistance; and Curtis Glavin for graphical design. We thank all patients and clinicians who contributed invaluable primary AML samples. This work was supported by the National Cancer Institute (NCI; 5K08 CA098444), the Howard Hughes Medical Institute, the Sidney Kimmel Cancer Foundation, the Claudia Adams Barr Foundation, and the Gloria Spivak Support Fund (K.S.).

Received: January 28, 2009
Revised: July 8, 2009
Accepted: August 19, 2009
Published: October 5, 2009

REFERENCES

Armstrong, S.A., Kung, A.L., Mabon, M.E., Silverman, L.B., Stam, R.W., Den Boer, M.L., Pieters, R., Kersey, J.H., Sallan, S.E., Fletcher, J.A., et al. (2003). Inhibition of FLT3 in MLL. Validation of a therapeutic target identified by gene expression based classification. Cancer Cell *3*, 173–183.

Balaian, L., and Ball, E.D. (2006). Cytotoxic activity of gemtuzumab ozogamicin (Mylotarg) in acute myeloid leukemia correlates with the expression of protein kinase Syk. Leukemia *20*, 2093–2101.

Boehrer, S., Ades, L., Braun, T., Galluzzi, L., Grosjean, J., Fabre, C., Le Roux, G., Gardin, C., Martin, A., de Botton, S., et al. (2008). Erlotinib exhibits antineoplastic off-target effects in AML and MDS: a preclinical study. Blood *111*, 2170–2180.

Braselmann, S., Taylor, V., Zhao, H., Wang, S., Sylvain, C., Baluom, M., Qu, K., Herlaar, E., Lau, A., Young, C., et al. (2006). R406, an orally available spleen tyrosine kinase inhibitor blocks fc receptor signaling and reduces immune complex-mediated inflammation. J. Pharmacol. Exp. Ther. *319*, 998–1008.

Burke, M.D., Berger, E.M., and Schreiber, S.L. (2003). Generating diverse skeletons of small molecules combinatorially. Science *302*, 613–618.

Chan, G., and Pilichowska, M. (2007). Complete remission in a patient with acute myelogenous leukemia treated with erlotinib for non small-cell lung cancer. Blood *110*, 1079–1080.

Chen, L., Monti, S., Juszczynski, P., Daley, J., Chen, W., Witzig, T.E., Habermann, T.M., Kutok, J.L., and Shipp, M.A. (2008). SYK-dependent tonic B-cell receptor signaling is a rational treatment target in diffuse large B-cell lymphoma. Blood *111*, 2230–2237.

Cheng, A.M., Rowley, B., Pao, W., Hayday, A., Bolen, J.B., and Pawson, T. (1995). Syk tyrosine kinase required for mouse viability and B-cell development. Nature *378*, 303–306.

Chu, D.H., Morita, C.T., and Weiss, A. (1998). The Syk family of protein tyrosine kinases in T-cell activation and development. Immunol. Rev. *165*, 167–180.

Deckert, M., Tartare-Deckert, S., Couture, C., Mustelin, T., and Altman, A. (1996). Functional and physical interactions of Syk family kinases with the Vav proto-oncogene product. Immunity *5*, 591–604.

Escudier, B., Eisen, T., Stadler, W.M., Szczylik, C., Oudard, S., Siebels, M., Negrier, S., Chevreau, C., Solska, E., Desai, A.A., et al. (2007). Sorafenib in advanced clear-cell renal-cell carcinoma. N. Engl. J. Med. *356*, 125–134.

Feldman, A.L., Sun, D.X., Law, M.E., Novak, A.J., Attygalle, A.D., Thorland, E.C., Fink, S.R., Vrana, J.A., Caron, B.L., Morice, W.G., et al. (2008). Overexpression of Syk tyrosine kinase in peripheral T-cell lymphomas. Leukemia *22*, 1139–1143.

Kanie, T., Abe, A., Matsuda, T., Kuno, Y., Towatari, M., Yamamoto, T., Saito, H., Emi, N., and Naoe, T. (2004). TEL-Syk fusion constitutively activates

PI3-K/Akt, MAPK and JAK2-independent STAT5 signal pathways. Leukemia *18*, 548–555.

Kimbrel, E.A., Davis, T.N., Bradner, J.E., and Kung, A.L. (2009). In vivo pharmacodynamic imaging of proteasome inhibition. Mol. Imaging. in press.

Kuno, Y., Abe, A., Emi, N., Iida, M., Yokozawa, T., Towatari, M., Tanimoto, M., and Saito, H. (2001). Constitutive kinase activation of the TEL-Syk fusion gene in myelodysplastic syndrome with t(9;12)(q22;p12). Blood *97*, 1050–1055.

Lamb, J., Crawford, E.D., Peck, D., Modell, J.W., Blat, I.C., Wrobel, M.J., Lerner, J., Brunet, J.P., Subramanian, A., Ross, K.N., et al. (2006). The Connectivity Map: using gene-expression signatures to connect small molecules, genes, and disease. Science *313*, 1929–1935.

Lindhagen, E., Eriksson, A., Wickstrom, M., Danielsson, K., Grundmark, B., Henriksson, R., Nygren, P., Aleskog, A., Larsson, R., and Hoglund, M. (2008). Significant cytotoxic activity in vitro of the EGFR tyrosine kinase inhibitor gefitinib in acute myeloblastic leukaemia. Eur. J. Haematol. *81*, 344–353.

List, A., Kurtin, S., Roe, D.J., Buresh, A., Mahadevan, D., Fuchs, D., Rimsza, L., Heaton, R., Knight, R., and Zeldis, J.B. (2005). Efficacy of lenalidomide in myelodysplastic syndromes. N. Engl. J. Med. *352*, 549–557.

List, A., Dewald, G., Bennett, J., Giagounidis, A., Raza, A., Feldman, E., Powell, B., Greenberg, P., Thomas, D., Stone, R., et al. (2006). Lenalidomide in the myelodysplastic syndrome with chromosome 5q deletion. N. Engl. J. Med. *355*, 1456–1465.

Lupher, M.L., Jr., Rao, N., Lill, N.L., Andoniou, C.E., Miyake, S., Clark, E.A., Druker, B., and Band, H. (1998). Cbl-mediated negative regulation of the Syk tyrosine kinase. A critical role for Cbl phosphotyrosine-binding domain binding to Syk phosphotyrosine 323. J. Biol. Chem. *273*, 35273–35281.

Moffat, J., Grueneberg, D.A., Yang, X., Kim, S.Y., Kloepfer, A.M., Hinkle, G., Piqani, B., Eisenhaure, T.M., Luo, B., Grenier, J.K., et al. (2006). A lentiviral RNAi library for human and mouse genes applied to an arrayed viral high-content screen. Cell *124*, 1283–1298.

Ong, S.E., Schenone, M., Margolin, A.A., Li, X., Do, K., Doud, M.K., Mani, D.R., Kuai, L., Wang, X., Wood, J.L., et al. (2009). Identifying the proteins to which small-molecule probes and drugs bind in cells. Proc. Natl. Acad. Sci. USA *106*, 4617–4622.

Peck, D., Crawford, E.D., Ross, K.N., Stegmaier, K., Golub, T.R., and Lamb, J. (2006). A method for high-throughput gene expression signature analysis. Genome Biol. *7*, R61.

Pitini, V., Arrigo, C., and Altavilla, G. (2008). Erlotinib in a patient with acute myelogenous leukemia and concomitant non-small-cell lung cancer. J. Clin. Oncol. *26*, 3645–3646.

Polo, J.M., Dell'Oso, T., Ranuncolo, S.M., Cerchietti, L., Beck, D., Da Silva, G.F., Prive, G.G., Licht, J.D., and Melnick, A. (2004). Specific peptide interference reveals BCL6 transcriptional and oncogenic mechanisms in B-cell lymphoma cells. Nat. Med. *10*, 1329–1335.

Ratain, M.J., Eisen, T., Stadler, W.M., Flaherty, K.T., Kaye, S.B., Rosner, G.L., Gore, M., Desai, A.A., Patnaik, A., Xiong, H.Q., et al. (2006). Phase II placebo-controlled randomized discontinuation trial of sorafenib in patients with metastatic renal cell carcinoma. J. Clin. Oncol. *24*, 2505–2512.

Rinaldi, A., Kwee, I., Taborelli, M., Largo, C., Uccella, S., Martin, V., Poretti, G., Gaidano, G., Calabrese, G., Martinelli, G., et al. (2006). Genomic and expression profiling identifies the B-cell associated tyrosine kinase Syk as a possible therapeutic target in mantle cell lymphoma. Br. J. Haematol. *132*, 303–316.

Rush, J., Moritz, A., Lee, K.A., Guo, A., Goss, V.L., Spek, E.J., Zhang, H., Zha, X.M., Polakiewicz, R.D., and Comb, M.J. (2005). Immunoaffinity profiling of tyrosine phosphorylation in cancer cells. Nat. Biotechnol. *23*, 94–101.

Sada, K., Takano, T., Yanagi, S., and Yamamura, H. (2001). Structure and function of Syk protein-tyrosine kinase. J. Biochem. *130*, 177–186.

Stegmaier, K., Ross, K.N., Colavito, S.A., O'Malley, S., Stockwell, B.R., and Golub, T.R. (2004). Gene expression-based high-throughput screening(GE-HTS) and application to leukemia differentiation. Nat. Genet. *36*, 257–263.

Stegmaier, K., Corsello, S.M., Ross, K.N., Wong, J.S., Deangelo, D.J., and Golub, T.R. (2005). Gefitinib induces myeloid differentiation of acute myeloid leukemia. Blood *106*, 2841–2848.

Stegmaier, K., Wong, J.S., Ross, K.N., Chow, K.T., Peck, D., Wright, R.D., Lessnick, S.L., Kung, A.L., and Golub, T.R. (2007). Signature-based small molecule screening identifies cytosine arabinoside as an EWS/FLI modulator in Ewing sarcoma. PLoS Med. *4*, e122.

Streubel, B., Vinatzer, U., Willheim, M., Raderer, M., and Chott, A. (2006). Novel t(5;9)(q33;q22) fuses ITK to SYK in unspecified peripheral T-cell lymphoma. Leukemia *20*, 313–318.

Stubbs, M.C., Kim, Y.M., Krivtsov, A.V., Wright, R.D., Feng, Z., Agarwal, J., Kung, A.L., and Armstrong, S.A. (2008). MLL-AF9 and FLT3 cooperation in acute myelogenous leukemia: development of a model for rapid therapeutic assessment. Leukemia *22*, 66–77.

Tomasson, M.H., Xiang, Z., Walgren, R., Zhao, Y., Kasai, Y., Miner, T., Ries, R.E., Lubman, O., Fremont, D.H., McLellan, M.D., et al. (2008). Somatic mutations and germline sequence variants in the expressed tyrosine kinase genes of patients with de novo acute myeloid leukemia. Blood *111*, 4797–4808.

Turner, M., Mee, P.J., Costello, P.S., Williams, O., Price, A.A., Duddy, L.P., Furlong, M.T., Geahlen, R.L., and Tybulewicz, V.L. (1995). Perinatal lethality and blocked B-cell development in mice lacking the tyrosine kinase Syk. Nature *378*, 298–302.

Turner, M., Schweighoffer, E., Colucci, F., Di Santo, J.P., and Tybulewicz, V.L. (2000). Tyrosine kinase SYK: essential functions for immunoreceptor signalling. Immunol. Today *21*, 148–154.

Vorhies, J.S., and Nemunaitis, J.J. (2009). Synthetic vs. natural/biodegradable polymers for delivery of shRNA-based cancer therapies. Methods Mol. Biol. *480*, 11–29.

Walensky, L.D., Kung, A.L., Escher, I., Malia, T.J., Barbuto, S., Wright, R.D., Wagner, G., Verdine, G.L., and Korsmeyer, S.J. (2004). Activation of apoptosis in vivo by a hydrocarbon-stapled BH3 helix. Science *305*, 1466–1470.

Weinblatt, M.E., Kavanaugh, A., Burgos-Vargas, R., Dikranian, A.H., Medrano-Ramirez, G., Morales-Torres, J.L., Murphy, F.T., Musser, T.K., Straniero, N., Vicente-Gonzales, A.V., et al. (2008). Treatment of rheumatoid arthritis with a syk kinase inhibitor: A twelve-week, randomized, placebo-controlled trial. Arthritis Rheum. *58*, 3309–3318.

Young, R.M., Hardy, I.R., Clarke, R.L., Lundy, N., Pine, P., Turner, B.C., Potter, T.A., and Refaeli, Y. (2008). Mouse models of non-Hodgkins lymphoma reveal Syk as an important therapeutic target. Blood *113*, 2508–2516.